ACS OMEGA

Open Access

http://pubs.acs.org/journal/acsodf

Article

Experimental Study and Molecular Dynamics Simulation of Oil Displacement Using Different Microemulsions in the Fang2 Block of Songfangtun Oilfield

Qi Zhang, Zhijun Zhou,* Xi Yi, Shuyang Wang, Aoxue Xing, and Chenzhu Wang

Cite This: *ACS Omega* 2024, 9, 48438−48451

Read Online

ACCESS | Metrics & More | Article Recommendations

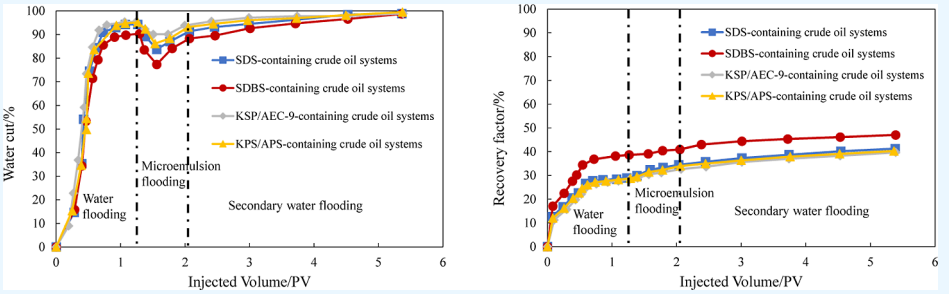

ABSTRACT: After many years of mining in the Fang2 block of the Songfangtun oilfield, the conventional water drive development method can no longer meet the requirement of greatly improving the recovery rate, and ternary composite drive (TCD) technology is adopted for this purpose. TCD is one of the most important methods to further improve crude oil recovery, and it has entered the industrialization and promotion stage, but there are still problems of fouling in the injection and extraction system and high production and maintenance costs. In order to reduce formation damage and improve recovery in the Songfangtun oilfield, an alkali-free microemulsion system was developed by replacing the weak base sodium carbonate with sodium chloride, but its emulsification capacity was weak and the recovery enhancement value was lower than that of the weak base TCD. In order to improve the emulsification performance of the alkali-free microemulsion and enhance the effect of oil repulsion, an alkali-free microemulsion oil-repellent system was developed on the basis of the alkali-free ternary system by using the compounding of surfactant, alcohol, and sodium chloride. Through indoor physical modeling experiments, it was concluded that the SDBS alkali-free microemulsion system had the best effect on improving crude oil rheology and viscosity reduction, and the lowest interfacial tension of 9.4×10^{-4} mN/m in the solution system when the mass fraction was 4%, with the maximum recovery rate of 47.03%, and the decrease in water content of 9.3%. Through molecular dynamics simulation and microemulsion oil-repellent coefficient, it is concluded that the alkali-free SDBS microemulsion system can greatly reduce the interaction force between crude oil and rock, with the lowest peak value of radial distribution function of 4.21, and the oil-repellent coefficient of F_p of 5.85; CMG reservoir numerical simulation software is adopted to verify the chemical repellent numerical simulation of Fang2 block, which shows that the recovery degree of SDBS alkali-free microemulsion system is 24.8% higher than that of water repellent, with the cumulative increase of 213.6 thousand tons of oil. The developed alkali-free microemulsion system not only realizes the goal of ternary composite alkalinity-free but also achieves the purpose of greatly improving the recovery rate and reducing the cost and increasing efficiency. It has a broad application prospect and can also provide a technical reference for the efficient development of other old oilfields with land-phase sandstone.

1. INTRODUCTION

Increased oil recovery has become more important due to the growth of oil and energy demand, resulting from rapid population growth and industrial economic development.[1] The oil extraction process is divided into three main phases: primary, secondary, and tertiary oil recovery phases. In the petroleum industry, primary and secondary oil recovery are known as conventional oil extraction methods, while tertiary oil recovery is referred to as enhanced oil recovery.[2,3]

Among them, ternary composite drive (TCD) is a highly efficient tertiary oil recovery technology, and field test results show that TCD can improve recovery by about 20% compared with water drive, and there is still room for improvement.[4] Compared with traditional polymer drives, TCDs include alkali

Received: July 26, 2024
Revised: November 13, 2024
Accepted: November 19, 2024
Published: November 26, 2024

https://doi.org/10.1021/acsomega.4c06741
ACS Omega 2024, 9, 48438−48451

and surfactant. It can adsorb on the rock surface while increasing the wave coefficient and drive crude oil out of the pores by changing the wettability of the rock and the ultralow interfacial tension between oil and water phases.[5,6] Ultralow interfacial tension usually relies on the coordinated action of alkali and surfactant, where the surfactant plays a key role. On the one hand, the special nature of surfactant molecules, with hydrophilic groups at one end and lipophilic nonpolar groups at the other end, forms a molecular film with directional distribution at the interface to reduce the interfacial tension,[7,8] and on the other hand, by varying the mass fraction of the surfactant, the ternary microemulsion composite system from the lower phase (Winsor type I) to the middle phase (Winsor type III) and then to the upper phase (Winsor type II), in which Winsor type III has a strong oil-enhancing ability,[9−11] while the alkali species are added to increase the stability of the microemulsion.[12,13] At the same time, the addition of alkali greatly increases the damage to the formation, resulting in a series of problems such as clay dispersion in the formation, transport leading to a reduction in formation permeability, alkali fouling leading to a decline in well production capacity, and difficulties in emulsion dewatering of recovered fluids,[14−16] which greatly increases the cost of TCD oil recovery. Therefore, there is an urgent need for an alkali-free ternary microemulsion system with good oil-repellent effect, low cost of chemicals, and less fouling. The composition of the alkali-free ternary microemulsion composite system is different from that of the traditional ternary composite system, and there are fewer studies on the oil-repellent effect and intermolecular interactions during the emulsification process. For this reason, indoor oil repulsion experiments and molecular dynamics simulations of the alkali-free ternary microemulsion system were carried out to clarify the repellent effect of the alkali-free ternary microemulsion system on crude oil and the characteristics of the transport principle of each agent.

In the alkali-free ternary microemulsion system, reducing or not using alkali can effectively slow the occurrence of corrosion and scaling. Liu et al. used NaCl instead of Na_2CO_3 and explained the mechanism of significantly improving the recovery rate of the composite system under the alkali-free condition at the ionic level, and the cost of the chemicals of the alkali-free system was 17.02% lower than that of the alkali system under the premise of the same effect of improving the recovery rate of 1%. Ternary core oil drive experimental recovery is 27.31% higher than water drive and 2.56% lower than weak base TCD.[17] Zheng et al. showed through visualization experiments and MD simulation results that surfactants can promote residual oil drive and improve residual oil mobility, in addition, the Marangoni effect generated by interfacial tension gradient can convert interfacial energy into drive kinetic energy through the emulsification of the oil−water interface, providing a new type of plugging agent and an effective cleaner for low recovery in multilayered nonhomogeneous reservoirs.[18] The rapid development of computer performance has brought new analytical tools from the molecular field, however, it is a major challenge to understand the interactions between oil and polymer−surfactant fluids and to elucidate the mechanisms behind the complex multicomponent interactions under reservoir conditions.[19] In this study, we first constructed a model of alkali-free ternary microemulsion system by different types of surfactant molecules, analyzed the oil repelling behavior of alkali-free microemulsion from a microscopic perspective, and validated the indoor simulation experiments, which can provide technological reference for the efficient development of the old oilfields in other land-phase sandstones.

2. EXPERIMENTAL SECTION

2.1. Materials and Instruments. Sodium dodecyl benzenesulfonate (SDBS), sodium dodecyl sulfonate (SDS), naphthenic alkyl petroleum sulfonate (KPS), sodium aliphatic alcohol ethoxylate carboxylate (AEC-9), sodium dodecyl polyoxypropylene sulfonate (APS), Nantong Runfeng Petrochemical Company Limited, Jiangsu Province, China; *n*-butanol (C_4H_9OH), AR Tianjin Tianli Chemical Reagent Company Limited, Tianjin; sodium chloride (NaCl), CP, (Tianjin Fuyu Fine Chemical Co.), CP, Tianjin Fuyu Fine Chemical Co., Ltd.; RH-20 rheometer, Shanghai Baosheng Industrial Development Co., Ltd.; JJ2000B Rotating Drop Full Scale Interfacial Tension Measuring Instrument, Shanghai Zhongchen Digital Technology Equipment Co.; degassed crude oil from Fang2 block of Songfangtun Oil Field, the properties of which are shown in Table 1; and the core is a natural core from Songfangtun Oil Field (core length 5.09 cm, diameter 2.5 cm, permeability 132.1 mD).

Table 1. Basic Properties of Crude Oil in Songfangtun Oilfield

property	data
density (t/m^3)	0.867
viscosity (mPa·s)	32.3−39.36
solidification point (°C)	37.0
wax content (%)	21.14
gum content (%)	16.45
saturates (%)	53.6
aromatics (%)	24.9
resins (%)	11.4
asphaltenes (%)	8.3
API (deg)	32.2

2.2. Complex Microemulsion Systems. In order to obtain a better alkali-free microemulsion oil-repellent system and prolong the mixed-phase repulsion process, it is necessary for the formation of microemulsions to require the smallest amount of surfactant while being able to adsorb different ions and chemicals in the system. Therefore, the hydrocarbon surfactant SDBS,[20] which has a better wetting effect, along with alcohols as cosurfactants and NaCl, was selected to constitute the microemulsions. These were then compared with three other microemulsion systems to achieve high and stable production in the Fang2 block of the Songfangtun oilfield.

2.2.1. Orthogonal Experimental Design. The system consisted of five components: crude oil, formation water, SDBS, *n*-butanol, and NaCl. The volume ratio of oil/water was fixed at 1:1. The concentration levels of SDBS, *n*-butanol, and NaCl were adjusted, and the volumes of the microemulsion phase as well as the residual oil and water phases were recorded to analyze the results of the orthogonal experiments in order to select the optimal ratio of the alkali-free microemulsion system.

2.2.2. Solubilization Parameters. After establishing a fixed oil/water volume ratio of 1:1, precise quantities of *n*-butanol and NaCl were employed to prepare SDBS solutions with varying concentrations. The resulting solution was thoroughly mixed using a magnetic stirrer and then allowed to equilibrate for 10 h at 45 °C in a thermostat until phase equilibrium was achieved. The volumes of each phase were recorded, and a graph

https://doi.org/10.1021/acsomega.4c06741
ACS Omega 2024, 9, 48438−48451

illustrating the relationship between the activator concentration and phase volume was plotted. Additionally, salinity versus phase volume and alcohol concentration versus phase volume graphs were constructed by using this methodology while keeping other components constant. For the purpose of this study, the solubilization parameter was defined as the amount of oil/water solubilized per unit mass of the surfactant

$$SP_W = \frac{V_W}{m_s} \quad (1)$$

$$SP_O = \frac{V_O}{m_s} \quad (2)$$

where SP_W/SP_O is the amount of solubilized water and oil, g·mL^{-1}; V_W, V_O is the volume of solubilized water and oil, mL; and m_s is the mass of surfactant, g.

2.3. Rheological Testing of the System. The rheological properties of crude oil and spiked crude oil were determined by using an RH-20 rheometer equipped with a coaxial cylinder system. Initially, the rheometer was calibrated against a blank crude oil sample to obtain its viscosity at 20 °C, measured at 41.02 mPa·s, with an error within the permissible range of 0.26%. Subsequently, both the crude oil and spiked crude oil underwent rheological testing at different temperatures under a specific shear rate, resulting in their respective rheological curves.

2.4. Interfacial Tension Testing. For the experiment, formation water from the Fang 2 block of the SongFangTun oil field was utilized as the solution and four microemulsion systems were evaluated. Initially, these solutions were introduced into sample tubes, followed by thorough stirring after the addition of crude oil. Subsequently, a resting period of 1 h was observed. The interfacial tension measurements were conducted at a temperature of 60 °C by using an interfacial tensiometer operating at 5000 rpm. Finally, the corresponding graphs depicting the interfacial tension were plotted.

2.5. Microscopic Emulsion Droplet Size Determination. The geological crude oil from the Fang 2 block and each microemulsion system solution were heated to 100 °C, and 50 mL of each was mixed in a ratio of 1:1. Subsequently, each mixed solution was added under an emulsifying stirrer, with the rotational speed set to 10 000 rpm and timed for 1 min. The microstructure of each microemulsion was then measured by selecting an appropriate scale.

2.6. Testing the Oil Displacement Effect of Microemulsion Systems. An oil-repellent test platform was built. The configured surfactant solution was placed in the beaker. The test temperature was set to 60 °C. The natural rock core was submerged in the beaker and connected the other end of the electronic scale through the balance. The leverage principle was used to amplify the signal and determine the amount of oil driven out of the beaker. This amount was recorded through the display of the electronic scale and calculated the effectiveness of each surfactant's oil-repellent properties.

$$\eta = \frac{m}{m_2 - m_1} \times 100\% \quad (3)$$

where η is the oil drive efficiency, %; m is the active agent oil drive, g; m_2 is the mass of the core plus crude oil after submergence, g; and m_1 is the dry weight of the core, g.

3. MOLECULAR SIMULATION

3.1. Modeling of the Crude Oil System. Based on the basic properties of crude oil in the Songfangtunfang 2 block, a crude oil system model matching Daqing crude oil was established using Materials Studio 2020 software. In developing the Daqing crude oil system model, the average molecular model of gums proposed by Márquez[21] and the asphaltene molecular model of Liaohe crude oil were utilized, as shown in Figure 1.

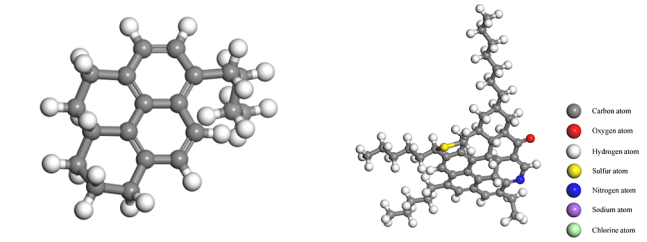

(a) Average molecular model of colloids (b) Asphaltene molecular model

Figure 1. Molecular model of the crude oil system.

The asphaltene and gum molecules in the crude oil system were created using the sketch tool, while C_8 was employed to establish the wax molecular model. Long-chain alkane molecules served as the molecular model for the saturated and aromatic fractions.

In the Construction tool of the Amorphous Cell module, periodic boundary conditions were applied to a periodic cubic box at 298 K. The box dimensions were 23.0 × 23.0 × 23.0 Å. Based on the proportions of the crude oil components presented in Table 1, the model of the crude oil system consisted of 4 gelatinous molecules, 1 asphaltene molecule, and 40 long-chain alkane model molecules. The crude oil system model is illustrated in Figure 2.

3.2. Molecular Modeling of Surfactants. The molecular structure was optimized under the Compass II force field using the Smart Minimize method to achieve energy minimization of the surfactant molecules see Figure 3.[22]

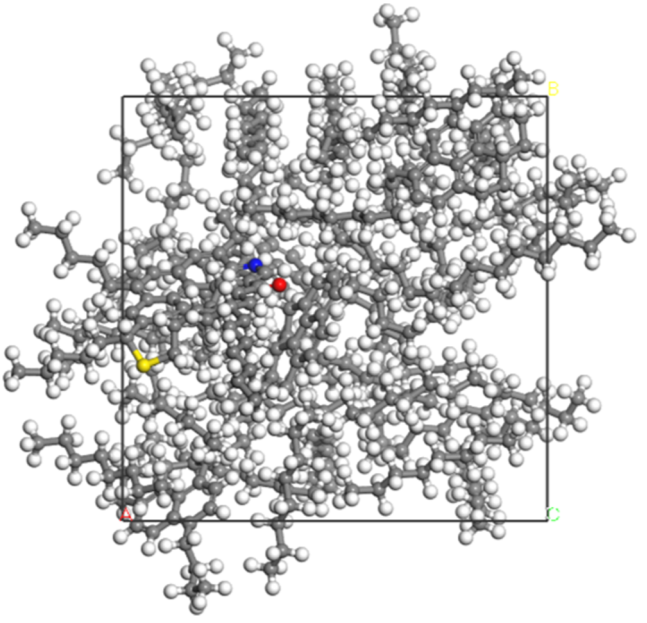

Figure 2. Crude oil system model of Songfangtunfang2 well area.

https://doi.org/10.1021/acsomega.4c06741
ACS Omega 2024, 9, 48438−48451

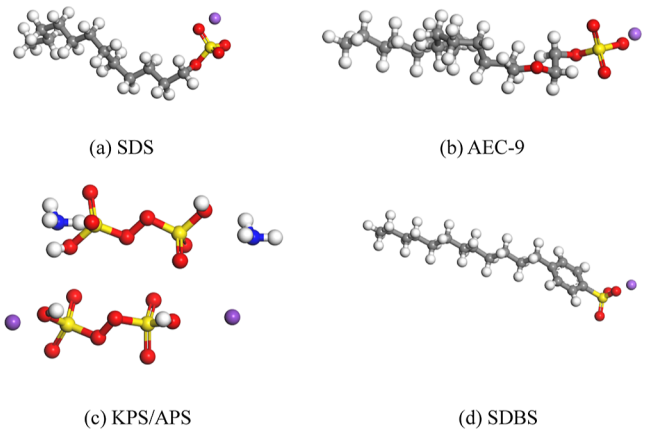

Figure 3. Molecular modeling of surfactants.

3.3. Molecular Dynamics Simulation. Based on molecular dynamics (MD) and Monte Carlo method,[23,24] simulations were carried out using Forcite, Amrophous cell module in MS (Materials Studio) 2020 software. First, using Construction in AC module, the optimized surfactant molecules were added to the stereocells according to the molar ratio of each system at the lowest energy of 1.061 g/cm^3 see Table 2, and the periodic boundary conditions were added, and then using Geometry Optimization in Forcite module, the Smart method was selected, and the optimization quality accuracy was fine, and the maximum iteration step was 5000 to obtain the optimized model with the lowest energy. The optimization mass accuracy is fine based on the Compass II force field, the maximum iteration step is 5000 for the geometry optimization to get the optimized model with the minimum energy, and finally the Dynamics tool is used for the calculations; the dynamics parameters are set as follows: the Compass II force field, NPT (constant temperature and pressure), the temperature is 298 K, the van der Waals force interaction, and electrostatic interactions. The atom-based method was used, and the temperature and pressure were controlled by an Anderson thermostat and a Berendsen constant pressure, respectively, to perform the kinetic simulations at 100 ps, simulating 10 000 steps with a time step of 1 fs.

Table 2. Molar Ratio of Components of Different Microemulsion Systems

systems	ingredient	molar mass (g/mol)	mole number (mol)	mole ratio
A	1.6% KPS/APS	342.23	0.0124	1:23.6
	5.8% NaCl	58.50	0.0237	
B	1.0% KPS	278.38	0.0360	1.44:1:6.76:23.96
	1.0% KPS/AEC-9	402.45	0.0250	
	1.25% C_4H_9OH	74.12	0.1690	
	3.5% NaCl	58.44	0.5990	
C	4.0% SDS	288.38	0.0147	1:6.8:2.6
	7.0% C_4H_9OH	74.12	0.1005	
	3.0% Na_2CO_3	105.99	0.0379	
D	4.0% SDBS	288.38	0.0147	1:6.5:0.6
	8.0% C_4H_9OH	74.12	0.0961	
	0.5% NaCl	58.44	0.0091	

Table 3. Results of Orthogonal Experiments

number	SDBS/ g·mL^{-1}	C_4H_9OH/ g·mL^{-1}	NaCl/ g·mL^{-1}	V_o/mL	V_w/mL	ΔV/mL
1	2.0	6.0	2.0	8.3	6.2	2.1
2	2.0	7.0	1.0	9.7	7.9	1.8
3	2.0	8.0	0.5	9.2	8.7	0.5
4	3.0	6.0	2.0	8.3	7.2	1.1
5	3.0	7.0	1.0	7.6	8.3	0.7
6	3.0	8.0	0.5	6.1	7.2	1.1
7	4.0	6.0	2.0	9.1	9.6	0.5
8	4.0	7.0	1.0	7.7	9.0	1.3
9	4.0	8.0	0.5	7.5	7.5	0.0

4. RESULTS AND DISCUSSION

4.1. Experimental Results. *4.1.1. Analysis of Orthogonal Experimental Results of the SDBS Alkali-Free Microemulsion System.* The above system D was optimized by orthogonal experiments[25] with component parameters, as shown in Table 3, and the volume difference $|V_o - V_w| = \Delta V$ between the remaining oil phase and the remaining water phase in the microemulsion system was used as a judgment indicator, the smaller ΔV was, the closer the system was to the optimal medium-phase microemulsion system.[26]

From Table 3, it can be seen that the best conditions for the optimal mesophase were C_{SDBS} = 4.0%, C_{C4H9OH} = 8.0%, and C_{NaCl} = 0.5%, using ΔV as a judgment indicator, and the influencing factors were *n*-butanol concentration, SDBS concentration, and NaCl concentration in the descending order.

4.1.2. Effect of SDBS System Composition on Phase and Solubilization Parameters. The oil/water volume ratio was maintained at 1:1 in the SDBS/alcohol/NaCl/crude oil/extracted water system at a temperature of 45 °C. By adjustment of the concentrations of SDBS, *n*-butanol, and NaCl, solubilization parameters were determined, as depicted in Figure 4.

At surfactant concentrations below the critical micelle concentration, the active agent is mainly concentrated at the oil−water interface and is used to reduce the interfacial tension.[27] Figure 4 illustrates that when SDBS concentrations exceed 0.4%, both SP_w and SP_o exhibit a rapid rise as the number of microemulsion aggregates increases. At a concentration of 4%, $SP_w = SP_o$, $\Delta V = 0$, indicating attainment of an optimal midphase state.

During the formation of alkali-free microemulsions, alcohols are partly involved in the formation of interfacial complex membranes and partly in the oil and aqueous phases making the improvement of the properties of both phases.[15,28] As can be seen from Figures 5 and 6, the midphase microemulsion starts to form when the *n*-butanol concentration reaches 5.3%. This is due to the fact that with the increase of *n*-butanol concentration, the charge density of the composite membrane decreases and it is easy to approach and agglomerate between the droplets, which makes the strength of the composite membrane increase, the SP_o increases, and the microemulsion-enriched phase separates from the lower phase to form the midphase. When the concentration was greater than 11.7%, *n*-butanol and SDBS began to enter the oil phase in large quantities, and the microemulsion in the middle phase was destroyed to form the microemulsion in the upper phase. The intersection of the SP_w and SP_o change curves was noted as SP* as an important indicator of the solubilizing ability of the microemulsion. The concentration corresponding

https://doi.org/10.1021/acsomega.4c06741
ACS Omega 2024, 9, 48438−48451

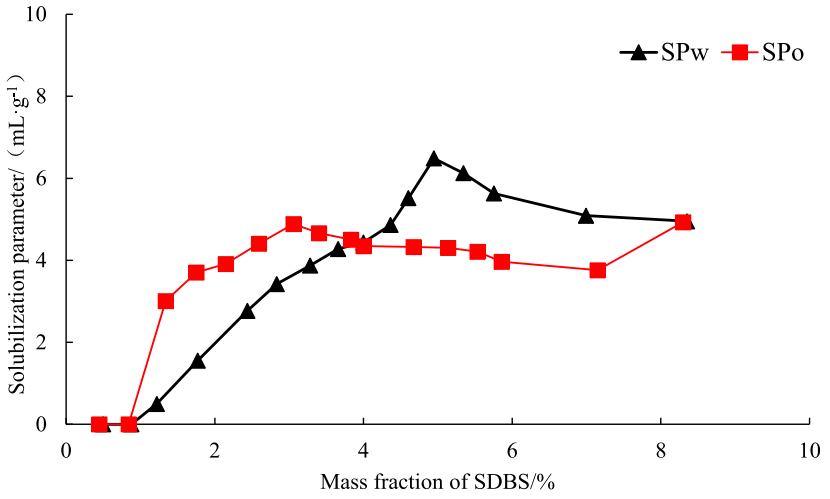

Figure 4. Effect of SBDS concentration on microemulsion.

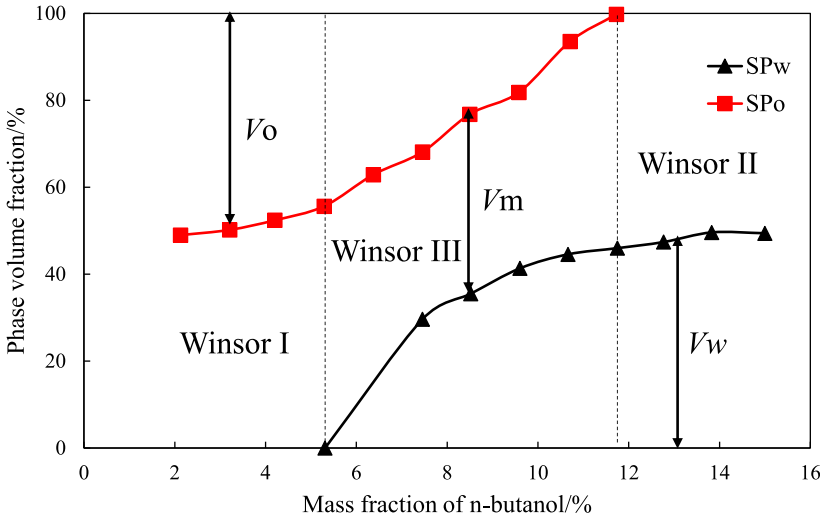

Figure 5. Effect of *n*-butanol on the volume mass fraction of each phase of microemulsion.

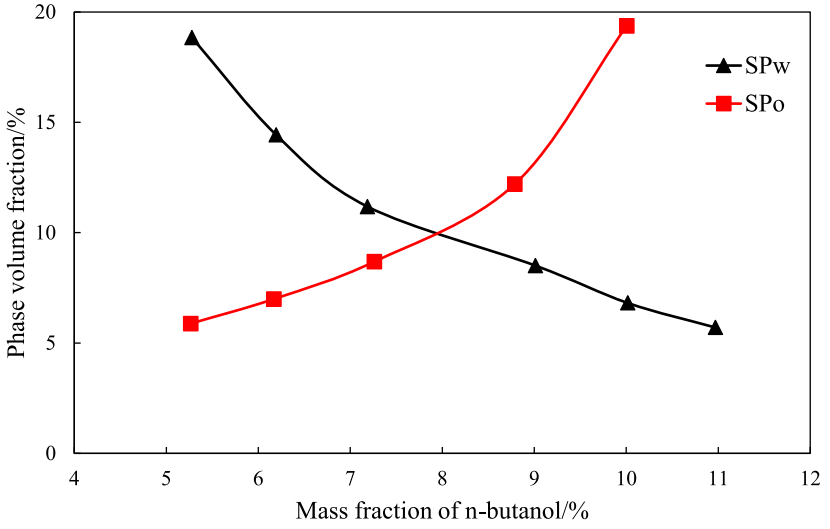

Figure 6. Effect of *n*-butanol concentration on solubilization parameters of microemulsions.

to SP* was called the optimal concentration; i.e., the optimal *n*-butanol of the system was 8.0%.

Changes in the NaCl concentration can speak of microemulsions changing from Winsor type I to Winsor type III, and NaCl has a dual effect on ionic surfactants: reducing the

https://doi.org/10.1021/acsomega.4c06741
ACS Omega 2024, 9, 48438−48451

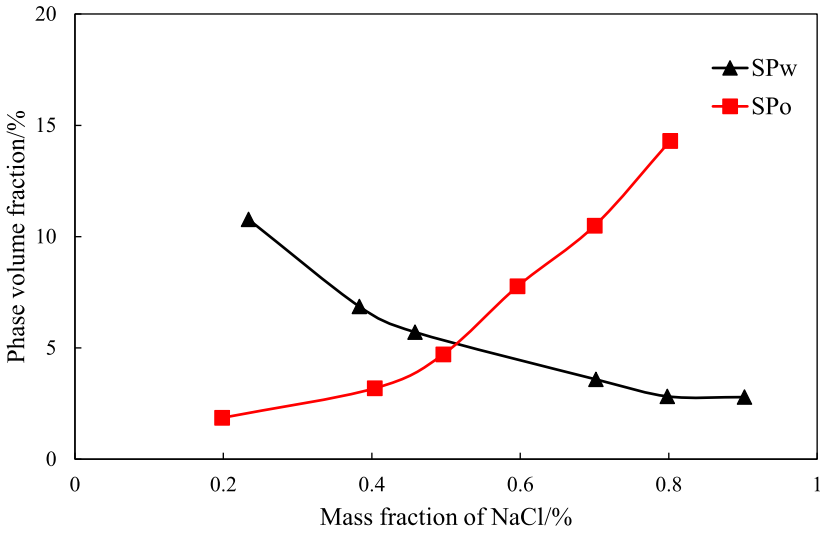

Figure 7. Effect of NaCl concentration on solubilization parameters of microemulsion.

Table 4. Variation of Viscosity of Blank Songfontein Crude Oil with Temperature and Shear Rate

	viscosity/(mPa·s)			
Temp/°C	10 s^{-1}	20 s^{-1}	30 s^{-1}	40 s^{-1}
70	36.2	36.2	36.2	36.2
60	51.3	51.3	51.3	51.3
50	65.1	65.1	65.1	65.1
45	86.9	86.9	86.9	86.9
40	198.3	187.9	179.2	175.4
35	265.1	259.3	250.7	241.9
30	498.2	465.2	411.2	409.6
25	612.3	593.8	540.6	500.7
20	822.0	776.5	732.9	714.3

repulsion between their hydrophilic headgroups and generating charged droplets during microemulsion formation.[29] As can be seen from Figure 7, with the increase in the NaCl concentration, the microemulsion system starts to solubilize the oil phase while releasing the water phase. SP_w gradually decreases, SP_o gradually increases, and the excess oil phase is gradually solubilized into the microemulsion system. The solubilization parameters of the oil and water phases in the figure intersected in the midphase region, with $SP_w = SP_o = SP^*$ at the intersection point, $\Delta V = 0$, corresponding to the optimal salinity of 0.5%.

4.1.3. Rheological Profiles of Different Microemulsions. The viscosity data of the blank crude oil and each microemulsion crude oil system were obtained using a RH-20 rheometer for determination. As shown in Table 4, the viscosity of the blank crude oil exhibited a gradual decrease with increasing temperature. Within the temperature range of 45−70 °C, there was no significant impact of shear rate on viscosity, indicating that the crude oil behaves as a Newtonian fluid in this range. Notably, an anomalous point at 45 °C was observed.

The viscosity−temperature curves of four different midphase microemulsion crude oil systems at a shear rate of 10 s^{-1} are compared in Figure 8. It can be observed that the viscosity of each microemulsion crude oil system decreases significantly with increasing temperature in the low-temperature range. However, as the temperature reaches 40 °C, the decrease rate of viscosity slows down. At low temperatures, strong nonbonding energy interactions between the molecules of crude oil components result in wax crystal precipitation and formation of a stable three-dimensional spatial mesh structure. These wax

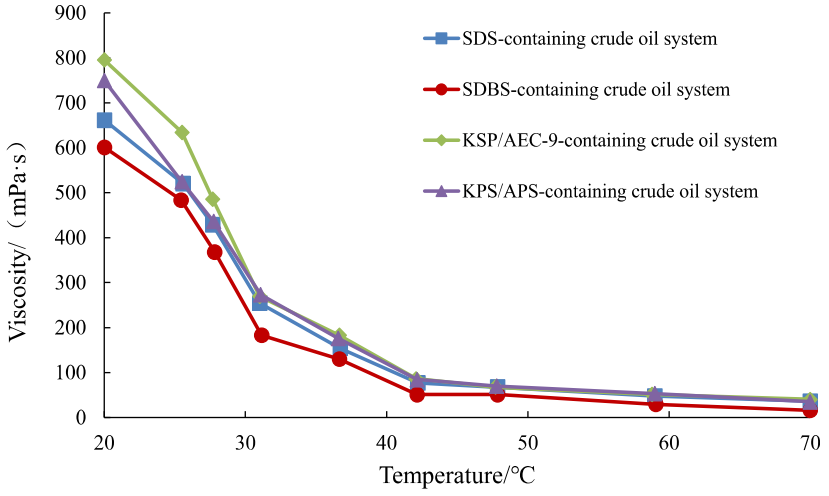

Figure 8. Comparison of viscosity−temperature curves of different microemulsion systems.

https://doi.org/10.1021/acsomega.4c06741
ACS Omega 2024, 9, 48438−48451

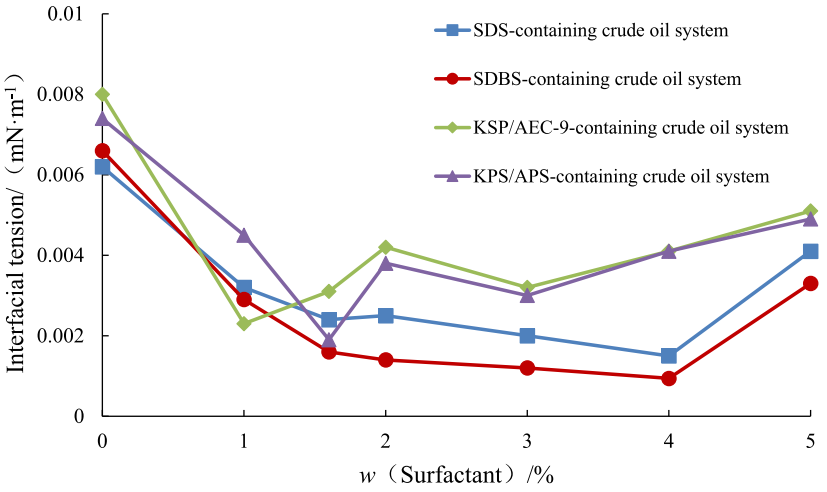

Figure 9. Comparison of interfacial tension of different microemulsion systems.

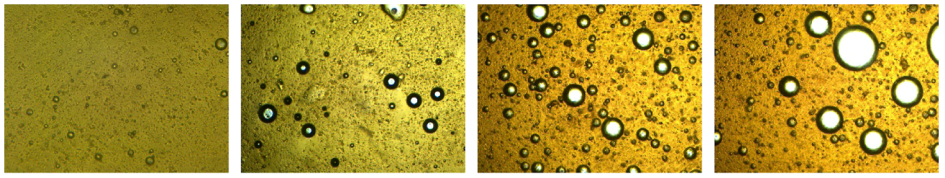

Figure 10. Observation of particle size of alkali-free microemulsion with different surfactants.

Table 5. Particle Size of Alkali-Free Microemulsions with Different Surfactants

serial number	surfactant	maximum size, μm	minimum size, μm	average size, μm
1	SDBS	3.25	0.43	1.35
2	SDS	4.32	0.49	1.81
3	KPS/APS	4.69	0.67	2.43
4	KPS/AEC-9	8.65	0.69	4.19

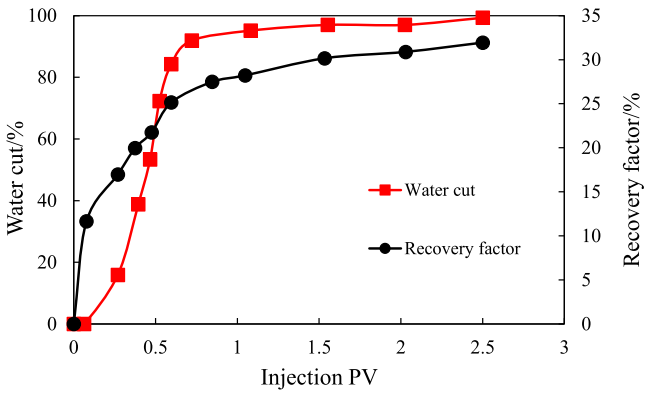

Figure 11. No. 1 core oil-repellent test results.

crystals adsorb low freezing point hydrocarbons, colloids, and asphaltenes to form a wax-like substance, causing loss of fluidity and higher viscosity in crude oil. As temperature gradually increases, nonbonding energy decreases, leading to dissolution of wax crystals and disruption of the stable network structure; simultaneously, the influence of colloids and asphaltenes on crude oil viscosity weakens, resulting in gradual decrease in viscosity. Addition of SDBS leads to maximum reduction in crude oil viscosity with the lowest value achieved at 20 °C. From the figure, it is evident that SDBS exhibits superior effect on reducing viscosity with order being SDBS > SDS > KPS/APS > KPS/AEC-9 system.

4.1.4. Interfacial Tension of Different Microemulsions with Crude Oil. Figure 9 illustrates the effect of the mass concentration of different microemulsion systems on interfacial tension. From the figure, it is evident that all four microemulsion systems exhibited good interfacial tension properties, indicating excellent interfacial stability for each mesophase microemulsion system. When the surfactant was the KPS/APS complex system, the lowest interfacial tension occurred at a mass fraction of 1.6%, measuring 1.9×10^{-3} mN/m. For the KPS/AEC-9 complex system, the lowest interfacial tension, 2.3×10^{-3} mN/m, was observed at a mass fraction of 1.0%. When SDS was used as the surfactant, the interfacial tension dropped to as low as 1.5×10^{-3} mN/m at a mass fraction of 4%. Finally, with SDBS as the surfactant, the lowest interfacial tension recorded was 9.4×10^{-4} mN/m at a mass fraction of 4%. Thus, the ability to reduce interfacial tension follows a descending order: SDBS > SDS > KPS/APS > and KPS/AEC-9.

4.1.5. Measurement of Emulsion Droplet Size of Different Microemulsions. In order to comprehensively analyze the microstructure of each alkali-free microemulsion, polarized light microscopy was employed to characterize its morphology. The microstructural results are shown in Figure 10, and the average size of the surfactant particles for each microemulsion is presented in Table 5. Compared to other microemulsion particle sizes, the average size of SDBS alkali-free microemulsions is the smallest at 1.35 μm. Microemulsions with smaller particle sizes tend to exhibit better stability and are more likely to penetrate rock pores, mixing with crude oil to form an easily flow able emulsion, thereby improving crude oil recovery.[30]

https://doi.org/10.1021/acsomega.4c06741
ACS Omega 2024, 9, 48438−48451

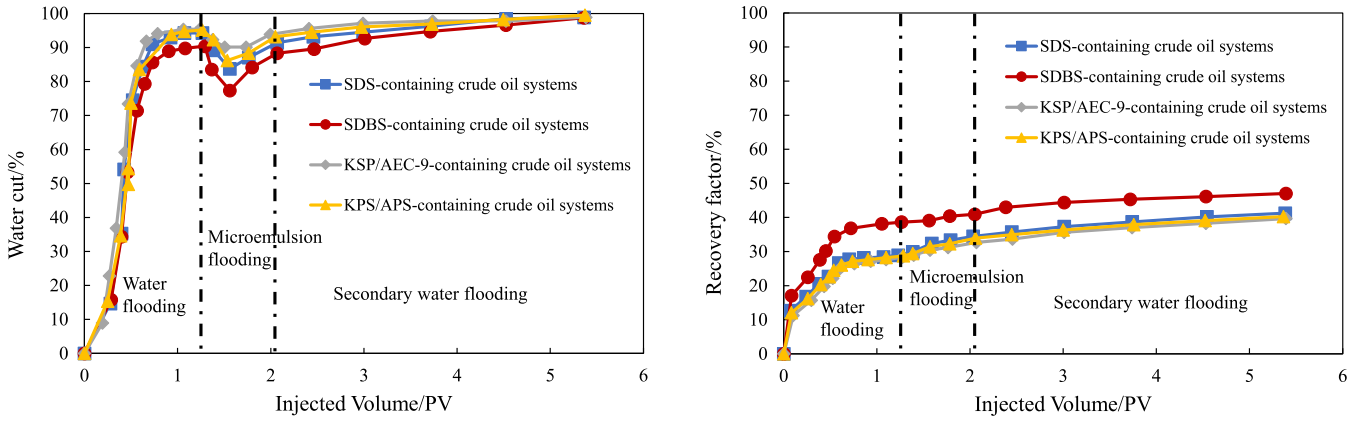

Figure 12. Results of oil-repellent test for each microemulsion system.

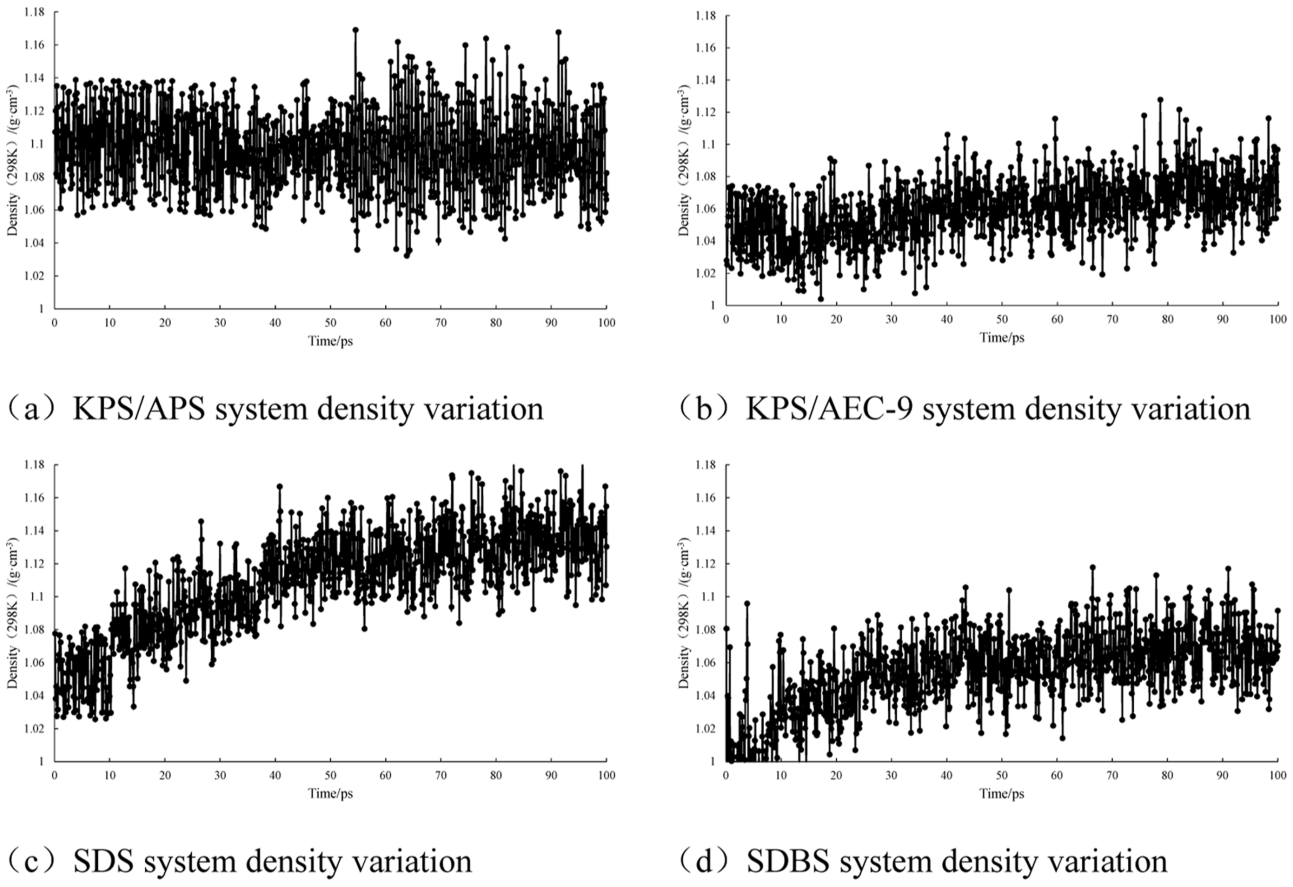

Figure 13. Density variation of different microemulsion systems.

4.1.6. Oil Repellent Effect of Different Microemulsions. Figures 11 and 12 present the results of oil repelling experiments conducted on different core samples: no.1 core (without additive), no.2 core (with KPS/APS compound system), no.3 core (with KPS/AEC-9 compound system), no.4 core (with the SDS system), and no.5 core (with SDBS). The introduction of microemulsion solutions resulted in increased oil recovery for all four of the treated core systems. Notably, the SDBS system exhibited the highest improvement, achieving a maximum recovery rate of 47.03%, which represents a 15.11% increase compared with the untreated core. Additionally, a decreasing trend in the water content was observed, with the SDBS system demonstrating the most significant reduction of 9.3%. These results indicate that the SDBS microemulsion system effectively reduces interfacial tension with oil, enhances the rheological properties of crude oil, facilitates the formation of a mixed phase with residual oil, and ultimately improves oil recovery rates.

4.2. Molecular Dynamics Simulation Results. *4.2.1. Comparison of Viscosity Reduction Effect of Different Microemulsion Systems.* Molecular dynamics simulations of the four established midphase microemulsion systems were performed by Materials Studio 2021 software. Figure 13 shows the density variation of each different midphase microemulsion crude oil system. In Dynamics, the equilibrium state of 100 ps was taken for analysis, and the simulated density (20 °C) of each system fluctuated in a small range around 1.061 g/cm^3. The

https://doi.org/10.1021/acsomega.4c06741
ACS Omega 2024, 9, 48438−48451

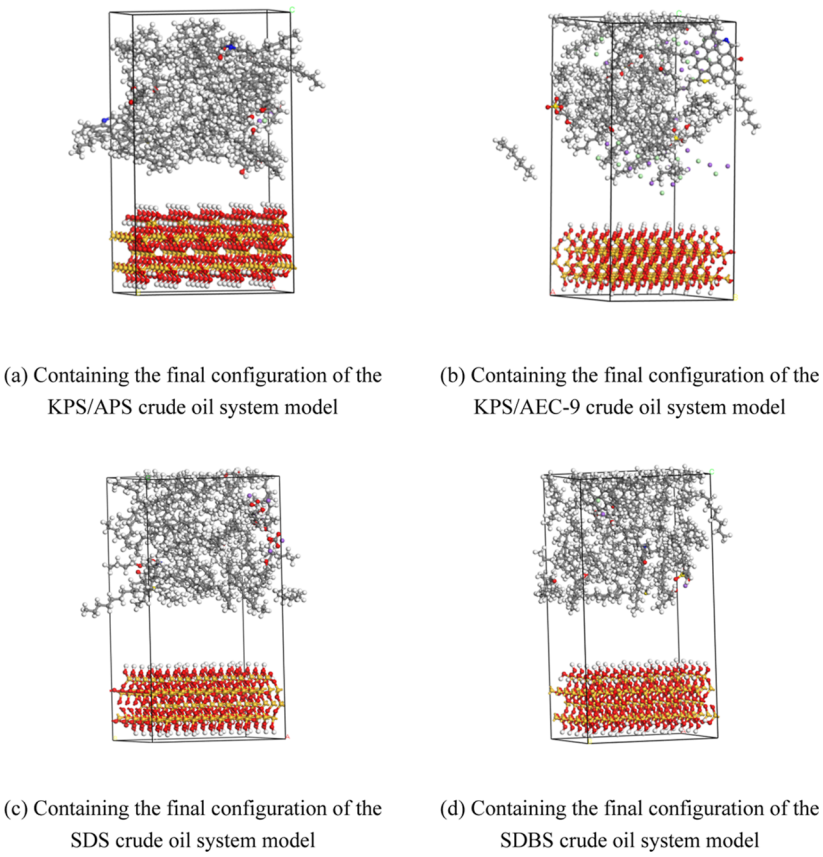

(a) Containing the final configuration of the KPS/APS crude oil system model

(b) Containing the final configuration of the KPS/AEC-9 crude oil system model

(c) Containing the final configuration of the SDS crude oil system model

(d) Containing the final configuration of the SDBS crude oil system model

Figure 14. Final configuration of different microemulsion crude oil system models.

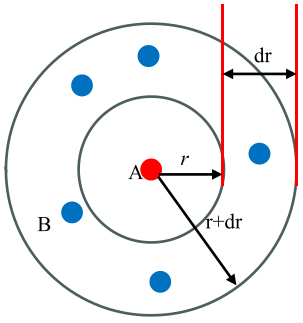

Figure 15. Schematic diagram of radial distribution of atoms.

different mesophase microemulsion systems were added to the crude oil system box with a box structure of 22.7 Å × 22.7 Å × 22.7 Å at 298 K by using the Construction tool in the Amorphous cell module, Periodic Cell periodic boundary conditions.

As shown in Figure 13, the density at 20 °C of the KPS/APS-containing system fluctuates within a small range around 1.055 g/cm^3; the density of the KPS/AEC-9-containing system fluctuates around 1.058 g/cm^3; the density of the SDS-containing system fluctuates around 1.052 g/cm^3; and the density of the SDBS-containing system fluctuates around 1.050 g/cm^3. Surfactant molecules adsorb onto the surface of wax crystals, disrupting the three-dimensional mesh structure formed by the wax crystals, which reduces the density of the system and leads to a decrease in crude oil viscosity.[31] Consequently, the viscosity reduction effects of the four microemulsion systems are ordered from high to low as follows: SDBS-containing system > SDS-containing system > KPS/APS-containing system > KPS/AEC-9-containing system.

4.2.2. Simulation of Microemulsion Oil-Repellent Effect. To ensure consistency between the simulation and experimental conditions, quartz was selected as the molecular model of the core to represent the sandstone formation, where Daqing crude oil is located. The Crystal tool under the Build module in MS software was utilized to select the P32 2 1 space group and input unit cell lattice parameters of 4.9134, 4.9134, and 5.4052, along with lattice angles of 90°, 90°, and 120° to create a new empty crystal cell. Subsequently, silicon and oxygen atoms were added using the Add Atoms tool to fill this empty cell and form a quartz structure. Finally, relaxation of the quartz (100) surface was performed through the supercell method using the Symmetry tool to generate a three-dimensional configuration.

The four types of microemulsion crude oil systems were modeled using quartz crystal cells through the Build Layers tool to establish a two-layer model. All models were subjected to a 100 ps molecular dynamics simulation, and the final configurations are shown in Figure 14. With the addition of different surfactants, a molecular film forms between the crude oil and the rock. This film reduces the surface tension between the liquid and solid as the surfactant adsorbs onto the rock surface, preventing direct contact between the crude oil molecules and the rock. Additionally, the surfactant in the microemulsion system alters the wettability of the crude oil and the rock, reducing the interaction force between the two. Furthermore, the anions in the surfactant can undergo ion exchange reactions with the cations on the rock surface, thereby weakening the adsorption between the crude oil and the rock. As a result, the crude oil molecules diffuse outward and gradually

https://doi.org/10.1021/acsomega.4c06741
ACS Omega 2024, 9, 48438−48451

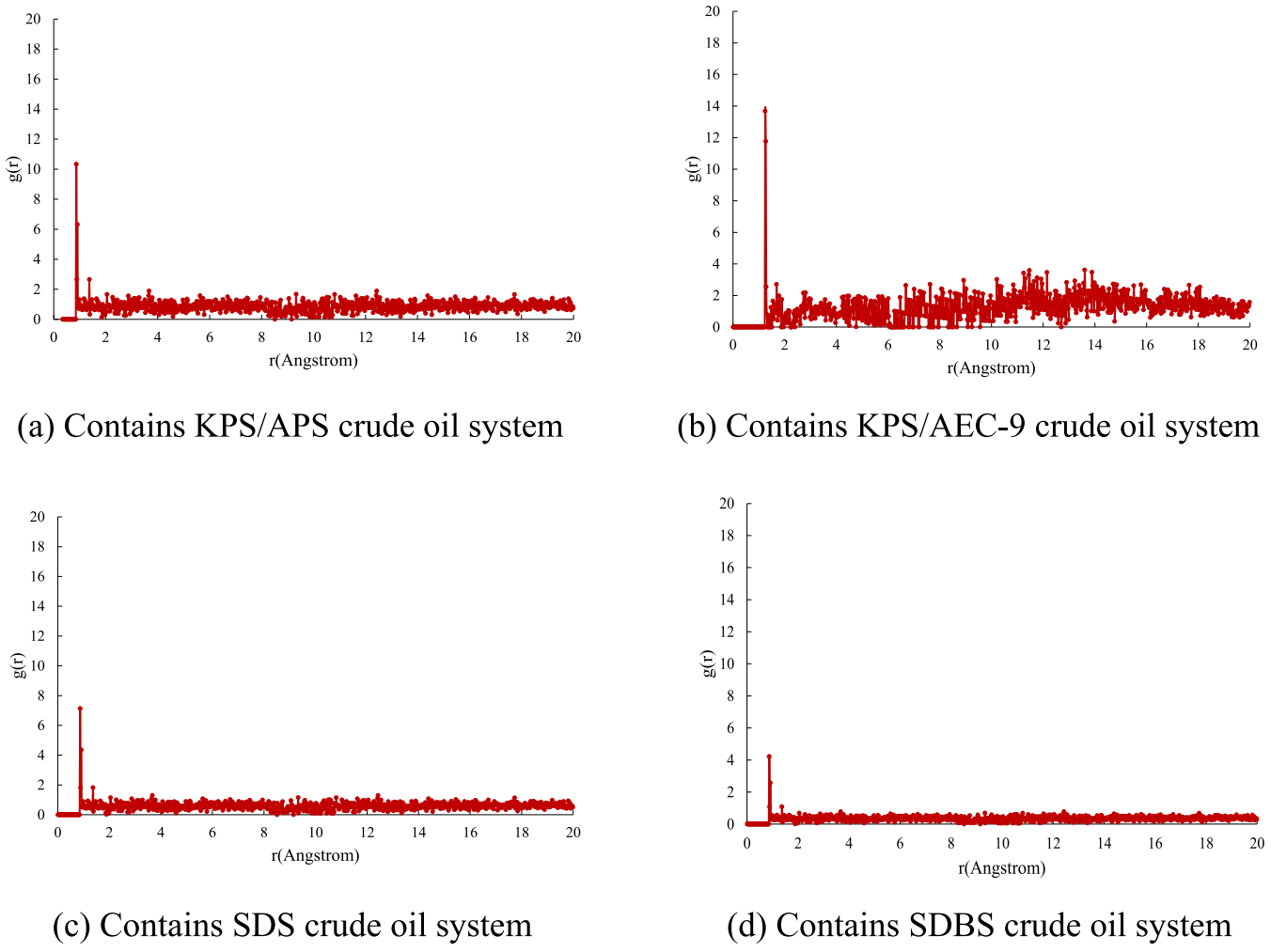

Figure 16. RDF curves of crude oil molecules versus rock for each microemulsion system.

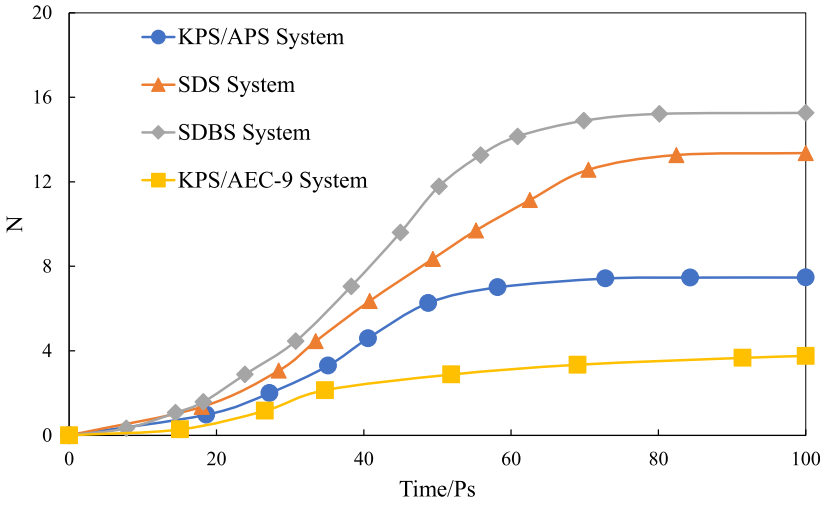

Figure 17. Variation in the number of *n*-octane hydrocarbon molecules entering the microemulsion system with time.

move away from the rock layer, achieving the effect of oil repulsion.[32,33]

To study the variation of the force exerted by crude oil molecules on the rock surface in different microemulsion systems, the final configuration of each microemulsion system shown in Figure 14 was analyzed using the Analysis tool of the Forcite module in MS to obtain the radial distribution function (RDF) of crude oil molecules with SiO_2 in each system.[34] The RDF represents the ratio of the central atom or molecule to other atoms or molecules separated by a certain distance, *r*, indicating the ratio of the local density to the average bulk density of the system, as illustrated in Figure 15.

https://doi.org/10.1021/acsomega.4c06741
ACS Omega 2024, 9, 48438−48451

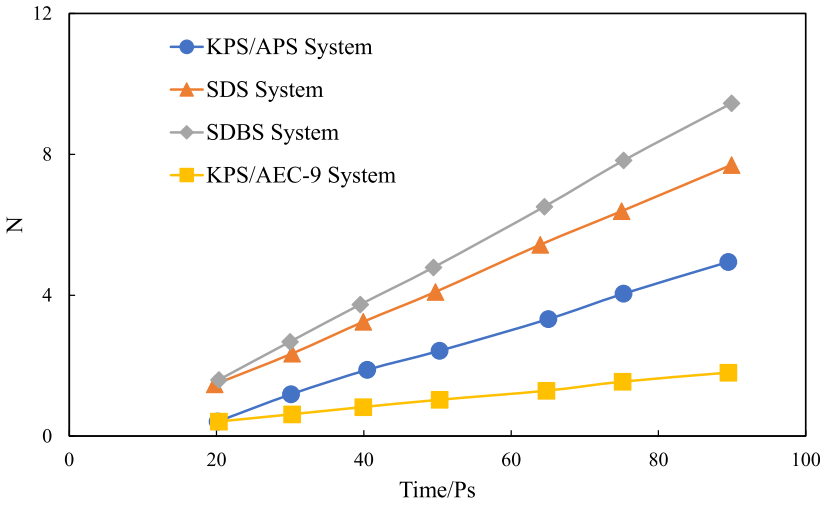

Figure 18. Rate of entry of *n*-octane into the microemulsion system.

Table 6. Comparison of Oil Repelling Ability of Different Microemulsion Systems

surfactant	interfacial tension/ mN m^{-1}	total potential energy/ 10^3 KJ·mol^{-1}	F_p/ps^{-1}
blank crude oil	7.02	−15.3	0
KPS/APS	1.9×10^{-3}	−17.2	3.71
KPS/AEC-9	2.3×10^{-3}	−16.4	3.62
SDS	1.5×10^{-3}	−18.9	5.23
SDBS	9.4×10^{-4}	−21.5	5.85

Table 7. Basic Parameters of Fang 2 Block

parameters	
porosity (%)	22.3
average penetration rate (mD)	231
average effective thickness (m)	2.3
oil saturation (%)	55.6
average saturation pressure (MPa)	4.44
original gas−oil ratio (m^3/t)	20.94
original ground pressure (MPa)	13.49
average stratigraphic temperature (°C)	63

With reference to the atom A as the center of the sphere, the number of atoms B in a thin spherical layer with radii ranging from r to $r + dr$, the number of atoms B is dN_{A-B} can be obtained, and the RDF $g_{A-B}(r)$ is defined as given by the following eq 4

$$g_{A-B}(r) = \frac{dN_{A-B}}{4\pi r^2 \rho_B dr} \tag{4}$$

$$dN_{A-B} = 4\pi r^2 \rho_B g_{A-B}(r) dr \tag{5}$$

where ρ_B denotes the number density of B atoms; r is the distance between A and B; and dN_{A-B} is the average number of B atoms present around A as a reference atom over the range of distances r to $r + dr$.

Through the RDF curve, the intuitive relationship between the interaction force of crude oil molecules and the SiO_2 surface can be established, allowing for an explanation of the microemulsion's oil-repelling effect from a micromechanical perspective. The peak value of the RDF curve represents the intensity of interactions between atoms at a given distance; a higher vertical coordinate $g(r)$ indicates a stronger interaction force between crude oil molecules and the rock surface, and vice versa. Figure 16 shows the RDF curve for each microemulsion

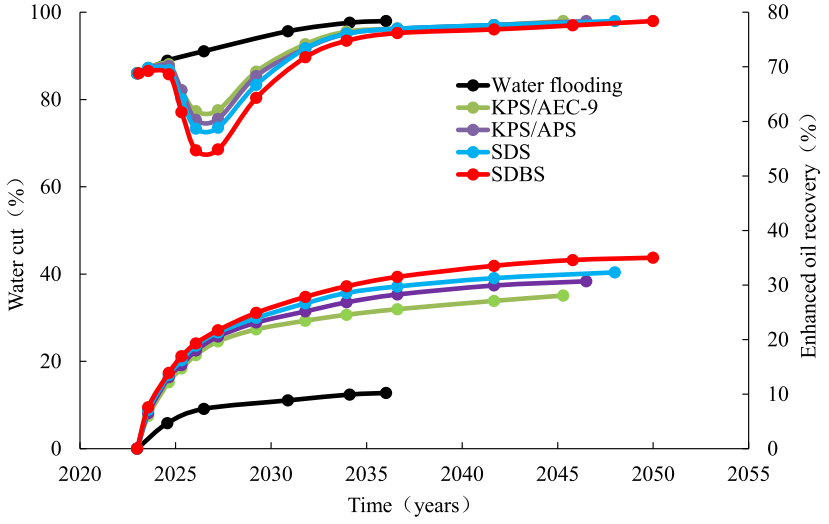

Figure 19. Relationship between water content and enhanced recovery for different systems.

https://doi.org/10.1021/acsomega.4c06741
ACS Omega 2024, 9, 48438−48451

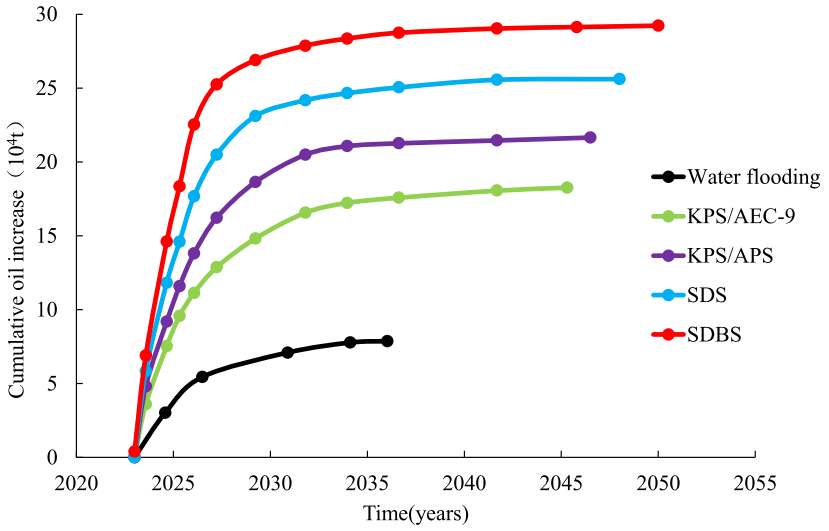

Figure 20. Cumulative oil gain of different systems.

crude oil system on the rock surface. It can be observed that the interaction between crude oil molecules and the rock surface varies across different microemulsion systems. The peaks for KPS/APS, KPS/AEC-9, SDS, and SDBS are 10.33, 13.67, 7.13, and 4.21, respectively. Notably, the four microemulsion systems exhibit strong interaction forces with the rock surface only in the early stage. In the middle and later stages, the distance between the crude oil molecules and the rock layer increases, indicating that the crude oil molecules move outward and that the microemulsion system effectively repels the oil. Among these, the RDF curve peak for the crude oil system containing SDBS is the smallest. From a microscopic perspective, the order of oil-repelling ability of the four microemulsions is as follows: SDBS > SDS > KPS/APS > KPS/AEC-9.

4.3. Relationship between *n*-Octane Molecular Number and Microemulsion Oil-Repellent Effect. The peak value of the RDF is used to express the oil-repellent effect of microemulsions in each system; however, this approach can be abstract and unintuitive. In this article, a more intuitive expression is proposed: the number of *n*-octane molecules entering the microemulsion system at different times serves as an indicator of the oil-repellent effect. Figure 17 shows that the numbers of *n*-octane molecules entering the KPS/APS system, the KPS/AEC-9 compound system, the SDS system, and the SDBS system at equilibrium are 6.46, 3.75, 13.36, and 15.25, respectively.

The number of *n*-octane molecules entering the aqueous phase at equilibrium can be considered a thermodynamic parameter.[35] From Figure 18, it can be observed that for the four microemulsion systems, the rate of *n*-octane molecules entering the oil-repellent system decreases in the following order: SDBS system, SDS system, KPS/APS system, and KPS/AEC-9 composite system.

4.4. Characterized Values of Microemulsion Oil-Repellency Coefficients. For a fixed molecular dynamics model, thermodynamic and kinetic factors should also be examined while using the number of *n*-octane molecules entering the aqueous phase at equilibrium or the diffusion rate to characterize the oil-repellent effect of microemulsions. Therefore, a new method to characterize the oil-repellent effect of microemulsion by combining the two is proposed, i.e., defining the microemulsion oil-repellent coefficient F_p as in eq 6

$$F_p = N \times (n/t) \tag{6}$$

where N represents the number of *n*-octane molecules entering the microemulsion system when the system reaches equilibrium, and n/t represents the rate of diffusion of *n*-octane molecules into the aqueous phase before reaching equilibrium.

The larger F_p indicates that the microemulsion oil-repellent effect is better. Comparison of the evaluation results of the microemulsion oil-repellent effect listed in Table 6 shows that the total potential energy of the SDBS system is the lowest and the most stable, and the maximum F_p is 5.85.

4.5. Numerical Simulation of SDBS Alkali-Free Microemulsion Oil Drive System. CMG numerical simulation software was used to predict the chemical drive scheme for the Songfangtun Fang2 block. The basic parameters of the block are shown in Table 7. There are 67 wells in the Fang2 block, including 52 oil recovery wells and 15 injection wells. Based on the original production well network and the injection–extraction relationship, the program predicts that from August 2023, with fixed liquid production, each system will reach an end water content of 98%. The cumulative oil increase, recovery degree, and water content are listed in Figures 19 and 20. The SDBS alkali-free microemulsion system improves the recovery degree by 24.8% compared to the water drive, resulting in a cumulative increase of 213.6 thousand tons of oil. The SDBS alkali-free microemulsion system not only significantly enhances the recovery degree but also eliminates scaling caused by alkali in the injection and recovery system, thereby reducing production management difficulties, maintenance workload, and operating costs. This approach achieves the goal of reducing costs and increasing efficiency through TCD.

5. CONCLUSIONS

(1) The main controlling factors for the formation of mesophase microemulsions by SBDS were known to be *n*-butanol concentration, SDBS concentration, and NaCl concentration by orthogonal experiments of solubilization parameters, and the solution showed Winsor type III when C_{SDBS} = 4.0%, $C_{n\text{-butanol}}$ = 8.0%, and C_{NaCl} = 0.5%, with $SP_w = SP_o = SP^*$, and $\Delta V = 0$.

(2) Through indoor physical experiments, the viscosity of crude oil with the addition of SDBS alkali-free micro-

https://doi.org/10.1021/acsomega.4c06741
ACS Omega 2024, 9, 48438−48451

emulsion decreased the most and showed the best viscosity reduction effect, with the lowest interfacial tension of 9.4×10^{-4} mN/m at 4% SDBS mass fraction, 47.03% recovery rate, and 9.3% reduction of water content; compared with the other four microstructures, the average particle size of SDBS solution was the smallest (1.35 μm).

(3) Through molecular dynamics simulation, the peak value of RDF of SDBS alkali-free microemulsion is 4.21, and the coefficient of oil repulsion of microemulsion is 5.85. This system not only reduces the interaction force between crude oil and rock surface but also accelerates significantly the speed of diffusion of crude oil into the aqueous phase; CMG numerical simulation software is used to predict that the degree of recovery of SDSB alkali-free microemulsion system is improved compared with water drive by 24.8%, and the cumulative oil increase is 213,600 tons.

AUTHOR INFORMATION

Corresponding Author

Zhijun Zhou − *Key Laboratory of Enhanced Oil Recovery, Northeast Petroleum University, Daqing, Heilongjiang 163000, China*; Email: sygc423@163.com

Authors

Qi Zhang − *Key Laboratory of Enhanced Oil Recovery, Northeast Petroleum University, Daqing, Heilongjiang 163000, China*; orcid.org/0009-0002-5836-1311

Xi Yi − *Civil Engineering and Architecture, Northeast Petroleum University, Daqing, Heilongjiang 163000, China*

Shuyang Wang − *Key Laboratory of Enhanced Oil Recovery, Northeast Petroleum University, Daqing, Heilongjiang 163000, China*

Aoxue Xing − *Key Laboratory of Enhanced Oil Recovery, Northeast Petroleum University, Daqing, Heilongjiang 163000, China*

Chenzhu Wang − *Key Laboratory of Enhanced Oil Recovery, Northeast Petroleum University, Daqing, Heilongjiang 163000, China*

Complete contact information is available at: https://pubs.acs.org/10.1021/acsomega.4c06741

Notes

The authors declare no competing financial interest.

ACKNOWLEDGMENTS

The research was supported by the China National Science and Technology Projects (2016ZX05012-002-002), the Northeast Petroleum University "National Fund" Foundation Project (2018GPYB-02), and the Postdoctoral Fund of Heilongjiang Province, under the project "Theoretical Model and Mechanism of Thick Oil SAGD Vapour Cavity Extension Based on Strongly Inhomogeneous Reservoirs" (LBH-Z23102).

REFERENCES

(1) Wang, Z.; Li, S.; Jin, Z.; Li, Z.; Liu, Q.; Zhang, K. Oil and gas pathway to net-zero: Review and outlook. *Energy Strat. Rev.* **2023**, *45*, 101048.

(2) Wang, X.; Gan, M.; Yang, X.; Zhang, P.; Peng, X.; Ju, Y.; Kou, Y.; Yu, X.; Zheng, L.; Wang, C. Mechanism of enhanced oil recovery by fuzzy-ball fluid as a novel oil-displacement agent. *Energy Rep.* **2023**, *9*, 1447−1463.

(3) Arain, A. H.; Negash, B. M.; Farooqi, A. S.; Alshareef, R. S. Improving Oil Recovery through Low Salinity Waterflooding and Nanoparticles: A Mini Review. *Energy Fuels* **2024**, *38*, 17109−17127.

(4) Mehraban, M. F.; Farzaneh, S. A.; Sohrabi, M. Debunking the Impact of Salinity on Crude Oil/Water Interfacial Tension. *Energy Fuels* **2021**, *35*, 3766−3779.

(5) Wang, W.; Peng, Y.; Chen, Z.; Liu, H.; Fan, J.; Liu, Y. Synergistic Effects of Weak Alkaline−Surfactant−Polymer and SiO2 Nanoparticles Flooding on Enhanced Heavy Oil Recovery. *Energy Fuels* **2022**, *36*, 7402−7413.

(6) Zhao, J.; Torabi, F.; Yang, J. The role of emulsification and IFT reduction in recovering heavy oil during alkaline-surfactant-assisted CO2 foam flooding: An experimental study. *Fuel* **2022**, *313*, 122942.

(7) Ghosh, S.; Ray, A.; Pramanik, N. Self-assembly of surfactants: An overview on general aspects of amphiphiles. *Biophys. Chem.* **2020**, *265*, 106429.

(8) Eskandar, N. G.; Simovic, S.; Prestidge, C. A. Interactions of hydrophilic silica nanoparticles and classical surfactants at non-polar oil−water interface. *J. Colloid Interface Sci.* **2011**, *358*, 217−225.

(9) Kittithammavong, V.; Charoensaeng, A.; Khaodhiar, S. Decontamination of oil-contaminated sand using anionic−nonionic mixed surfactant-based microemulsion formation: the study of surfactant and oil balances. *Int. J. Environ. Sci. Technol.* **2024**, *21*, 5395−5410.

(10) Wang, B.; Wang, X.; Hu, F.; Wang, X.; Yang, Z.; Zhu, X.; Li, G.; Wang, K. Study on the Properties of Compound Surfactants with PO Groups. *Energies* **2024**, *17*, 513.

(11) Hu, H.; Zhang, Q.; Tian, M.; Li, Y.; Han, X.; Guo, R. Review: Microemulsions for the Sustainable Development of EOR. *Sustainability* **2024**, *16*, 629.

(12) Cao, G.; Du, T.; Bai, Y.; Yang, T.; Zuo, J. Effects of surfactant molecular structure on the stability of water in oil emulsion. *J. Pet. Sci. Eng.* **2021**, *196*, 107695.

(13) McClements, D. J.; Jafari, S. M. Improving emulsion formation, stability and performance using mixed emulsifiers: A review. *Adv. Colloid Interface Sci.* **2018**, *251*, 55−79.

(14) Chung, J.; Holtsclaw, J.; Henderson, T. C.; Everett, T. A.; Schultheiss, N. C.; Boudouris, B. W.; Franses, E. I. Relationship of Various Interfacial Tensions of Surfactants/Brine/Oil Formulations to Oil Recovery Efficiency. *Energy Fuels* **2021**, *35*, 7768−7777.

(15) Wu, J.; Mei, P.; Lai, L. Microemulsion and interfacial properties of anionic/nonionic surfactant mixtures based on sulfonate surfactants: The influence of alcohol. *J. Mol. Liq.* **2023**, *371*, 120814.

(16) Tackie-Otoo, B. N.; Atta, D. Y.; Ayoub Mohammed, M. A.; Otchere, D. A. Investigation into the Oil Recovery Process Using an Organic Alkali−Amino Acid-Based Surfactant System. *Energy Fuels* **2021**, *35*, 11171−11192.

(17) Liu, X.; Wu, H.; Chen, S.; He, J.; Yang, Z.; Cheng, J.; Wu, J. Study on the Alkali-Free Three-Component Flooding System in the Daqing Oilfield. *ACS Omega* **2024**, *9*, 16006−16015.

(18) Zheng, H.; Liu, H.; Tong, K. Insights into Molecular Dynamics and Oil Extraction Behavior of the Polymeric Surfactant in a Multilayered Heterogeneous Reservoir. *ACS Omega* **2024**, *9*, 11243−11254.

(19) Sun, H.; LiLiu, X. D.; Li, X.; Li, X. Synergetic adsorption of asphaltenes and oil displacement surfactants on the oil-water interface: Insights on stabilization mechanism of the interfacial film. *Chem. Eng. Sci.* **2021**, *245*, 116850.

(20) Barari, M.; Lashkarbolooki, M.; Abedini, R.; Hezave, A. Z. Effects of conventional and ionic liquid-based surfactants and sodium tetraborate on interfacial tension of acidic crude oil. *Sci. Rep.* **2024**, *14*, 2618.

(21) Márquez, M. L.; Rogel, E.; Reif, I. Molecular dynamics simulation of isopropyl naphthalene sulfonate at the water/heptane interface. *Colloids Surf., A* **1996**, *106*, 135−148.

(22) Reil, M.; Hoffman, J.; Predecki, P.; Kumosa, M. Intermolecular interactions in graphene and oxidized graphene nanocomposites. *Compos. Sci. Technol.* **2024**, *248*, 110433.

(23) Hao, T.; Jiang, S.; Wang, L.; Jiang, W. Experimental and molecular dynamics simulation study of the effect of composite surfactants on wetting of coal dust. *J. Mol. Liq.* **2024**, *409*, 125552.
(24) Wang, K.; Xu, M.; Zhou, B.; Yang, M.; Liu, R. Study on the effects of inorganic salts and ionic surfactants on the wettability of coal based on the experimental and molecular dynamics investigations. *Energy* **2024**, *300*, 131610.
(25) Zheng, M.; Yu, J. Probabilistic approach for robust design with orthogonal experimental methodology in case of target the best. *J. Umm Al-Qura Univ. Eng. Archit.* **2024**, *15*, 55−59.
(26) Jiang, Z.; Liu, T.; Zhai, X.; Liu, J. Optimization Preparation of Indium Tin Oxide Nanoparticles via Microemulsion Method Using Orthogonal Experiment. *Crystals* **2021**, *11*, 1387.
(27) Ogunmokun, F. A.; Wallach, R. Effect of surfactant surface and interfacial tension reduction on infiltration into hydrophobic porous media. *Geoderma* **2024**, *441*, 116735.
(28) Qi, W.; Deng, Q.; Du, N.; Hou, W. Surfactant-free microemulsions of n-butanol, ethanol, and water. *J. Mol. Liq.* **2023**, *390*, 122980.
(29) Leng, K.; Guan, B.; Liu, W.; Jiang, C.; Cong, S.; Peng, B.; Tao, Y. Advance of Microemulsion and Application for Enhanced Oil Recovery. *Nanomaterials* **2024**, *14*, 1004.
(30) Liu, Z.; Liu, P.; Shi, D.; Gao, Y.; Hei, Y.; Guo, F.; Li, X.; Leng, W.; Xie, Q.; Lv, Q.; Sun, W. Revealing the microscopic formation mechanism and stability characteristics of anionic surfactant microemulsions using coarse-grained simulations. *Chem. Eng. Sci.* **2024**, *285*, 119570.
(31) Chen, X.; Li, C.; Liu, D.; Li, B.; Zhang, H.; Yang, F.; Sun, G.; Dai, S.; Zhao, Y. Effect of doped emulsifiers on the morphology of precipitated wax crystals and the gel structure of water-in-model-oil emulsions. *Colloids Surf., A* **2020**, *607*, 125434.
(32) Obuebite, A. A.; Okwonna, O. O.; Eke, W. I.; Akaranta, O. Orange Mesocarp Extract as a Natural Surfactant: Impact on Fluid−Fluid and Fluid−Rock Interactions during Chemical Flooding. *ACS Omega* **2024**, *9*, 4263−4276.
(33) Khosravani, M.; Akhlaghi, N.; Hosseini, S. Investigation of ionic liquid adsorption and interfacial tension reduction using different crude oils; effects of salts, ionic liquid, and pH. *Sci. Rep.* **2024**, *14*, 10720.
(34) Neyts, E. C.; Bogaerts, A. Combining molecular dynamics with Monte Carlo simulations: implementations and applications; Champagne, B., Deleuze, M. S., De Proft, F., Leyssens, T., Eds.; Springer Berlin Heidelberg: Berlin, Heidelberg, 2014; pp 277−288.*Theoretical Chemistry in Belgium: A Topical Collection from Theoretical Chemistry Accounts*
(35) Abdi, M.; Hassanzadeh, H. Thermodynamic study of water/solvent, bitumen/solvent, water/bitumen, and water/bitumen/solvent systems: From CPA EoS parametrization towards phase diagram construction. *Fuel* **2024**, *378*, 132821.

https://doi.org/10.1021/acsomega.4c06741
ACS Omega 2024, 9, 48438−48451